A Novel Three-Dimensional Coordinate Positioning Algorithm Based on Factor Graph

QIANG HAO[1], YA ZHANG[1], SHIWEI FAN[1], PAN JIANG[1], HONGLIANG YIN[2], AND DINGJIE XU[1]

[1]School of Instrumentation Science and Engineering, Harbin Institute of Technology, Harbin 150001, China
[2]China Ship Research and Development Academy, Beijing 100192, China

Corresponding author: Ya Zhang (yazhang@hit.edu.cn)

ABSTRACT In this paper, a novel three-dimensional coordinate positioning algorithm based on factor graph is proposed to improve the measurement accuracy of the indoor global positioning system (iGPS) under large scale conditions. Different from the traditional iGPS positioning algorithm based on the least squares estimation, which has the problems of fixed solution model, low confidence results and poor stability, this proposed algorithm utilized Bayesian filtering to solve the coordinate positioning problem. Aiming at the character of plug and play for iGPS, a factor graph model based on Bayesian network is built, and then a sum product algorithm is used to convert the fixed model into the form of the product of every node, which reduces the independence of measurement information, and improves the confidence of the results. Furthermore, to further improve the positioning accuracy of the algorithm, an idea of maximum posterior estimation is integrated into the proposed algorithm, which enhances the stability of the algorithm at the same time. In order to verify the effectiveness of the proposed algorithm, a series of simulation and prototype tests have been carried out. The results show that compared with the traditional positioning algorithm based on least squares estimation, the accuracy of the proposed algorithm is improved by about 50%, and the positioning accuracy can achieve 0.3mm within a range of 10 meters, which realizes a high-precision measurement under large scale conditions.

INDEX TERMS Coordinate positioning, factor graph, least squares estimation, indoor global positioning system, laser scan.

I. INTRODUCTION

There are many different indoor positioning technologies, such as wireless fiedelity (WiFi), bluetooth, radio frequency identification (RFID), Zigbee, inertial measurement units (IMU), visible light positioning (VLP) and so on, which are the hotspots research at home and abroad. Among them, WiFi, bluetooth, RFID and Zigbee have a positioning accuracy in meter level, and there are some problems such as low positioning accuracy, many signal access points and low system stability [1]–[4]; IMU has a high positioning accuracy in a short time, but due to the influence of gyro

drift and accelerometer zero deviation, the positioning error increases with the increase of time [5], [6]; VLP has the positioning accuracy of centimeters or even millimeters and has good long-term stability, which shows a bright futrue for VLP [7]–[9].

However, in the large equipment manufacturing projects, the three-dimensional (3D) positioning accuracy requirements usually can be reached at a level of millimeter or even sub-millimeter in a few tens of meters of space [10]–[12]. As a result, the indoor positioning technologies as mentioned above cannot be suitable for the precision measurement under such conditions. To solve this problem, laser tracker, total station, theodolite and other new optical measuring facilities have been developed and applied in many technological

The associate editor coordinating the review of this manuscript and approving it for publication was Walter Didimo[ID].

stages such as parts assembly, tunneling and deformation measurement for aircraft, subway and shipbuilding [13]–[15]. However, limited to the working principle of the facilities, they need a long time to achieve one single point positioning, which is quite low-efficient.

In order to realize the 3D coordinates output in millimeter level, high efficiency and large scale conditions, NiKon proposed a new spatial measurement and positioning system called indoor global positioning system (iGPS), also Tian-Jin University invented a similar system called workspace measurement positioning system (wMPS) [16]–[19]. These systems realize positioning through the principle of angle intersection measurement based on laser scan; Furthermore, with the help of high-speed rotating motor, the systems can scan the measured space with a high frequency, and carry out a high frequency position information output. Based on the above two points, the systems solve the problem of low measurement efficiency under the condition of high positioning accuracy. Now these systems have been used as a new measurement method in many measurement and positioning scenarios. From the above, to enhance the systems' positioning capability, improve the precision level of large-scale equipment manufacturing, it is of great significance to carry out in-depth research on these systems, especially the research on positioning algorithm.

According to Reference [20], these systems construct the constraint equations through the bundle adjustment method based on photogrammetry at first, and then use the least square estimation (LSE) to acquire the 3D coordinates. This positioning algorithm is quite simple and easy to implement, however, there are three problems for it.

(1) The algorithm mathematical model is fixed. Due to the plug and play characteristics of these systems, the number of transmitter may change during measurement and this will directly cause a change in the algorithm mathematical model, resulting in abnormal positioning solution of these systems and affecting the positioning effect;

(2) The positioning results are independent of each other with poor correlation. According to the algorithm mathematical model, once the number of observation information meets the demand of LSE model, the positioning solution is carried out, and the 3D positioning coordinates are output. However, since the observation information is not related to each other, the solution result is independent, which reduces the confidence of the positioning result and causes the resource waste of observation information.

(3) The algorithm based on LSE has weak anti-interference ability. Because of the poor robustness of LSE, when the system is disturbed, such as external vibration or speed mutation, its observation information will be mixed with errors, and these mixed errors will accompany in the solution process. As a result, the final positioning accuracy is decreased.

Due to the specificity and particularity of iGPS and wMPS, few people have carried out relevant algorithm optimization research on above problems. In this paper, a 3D coordinate positioning method based on factor graph (FG) is

proposed to solve these problems. At first, based on the idea of factor graph and sum-product, we regard this observation information as a series of independent local nodes, thus the fixed mathematical model can be changed into the product of local nodes [21]. Thanks to the feature of flexible configuration for local nodes, the proposed algorithm can realize plug and play of observation information, and can no longer be limited to fixed mathematical models; Then since each independent local node is connected by soft message, thus a Bayesian network which satisfies the Markov process is formed, which improves the correlation of positioning estimation and improves the confidence of measurement results [22]; Besides, based on the thought of maximum posteriori estimation criterion, the proposed algorithm updates the state information at first and then the measurement information, which improve the robustness of the algorithm.

The remainder of this paper is organized as follows: Section 2 introduces the working principle and the accurate mathematical model. Section 3 designs the 3D coordinate positioning method based on FG. A validity evaluation is presented in section 4, including simulation and prototype tests. At last, a conclusion is remarked in section 5.

II. WORKING PRINCIPLE
A. SYSTEM COMPONENTS
The main components of iGPS and wMPS are shown as Fig.1. The receiver placed in the point to be measured is a photoelectric converter, and it can receive optical signals from the transmitters and send the converted electrical signals to the front-end processor. The working principle of transmitter is similar to a theodolite to some extent, which measures the receiver's azimuth and pitch angles relative to itself [23]. Specifically, two line lasers with a fixed angle (θ_{off}) emit two fanned laser planes, and the two fanned laser planes can sweep through the whole measured space at a constant speed (ω) with the help of a stepping motor. Once the laser plane **1** turns a circle, the pulse lasers deliver pulse singles to receivers as the transmitter's starting time (T_0). The front-end processor separates the received signals from the line lasers and the pulse lasers, and calculates the time (T_1, T_2) when the receiver receives the signal from the two line laser. As a result, the scanning angles (θ_1, θ_2) of the two laser planes can be calculated based on the rotating speed (ω), shown as Equation (1). Based on the scanning angles, the receiver's coordinates can be determined as long as the receiver receives signals from at least two transmitters. Finally, to display the 3D coordinates, the results are sent to the computer through WiFi.

$$\begin{cases} \theta_1 = \omega\,(T_1 - T_0) \\ \theta_2 = \omega\,(T_2 - T_0) \end{cases} \tag{1}$$

B. MATHEMATICAL MODEL
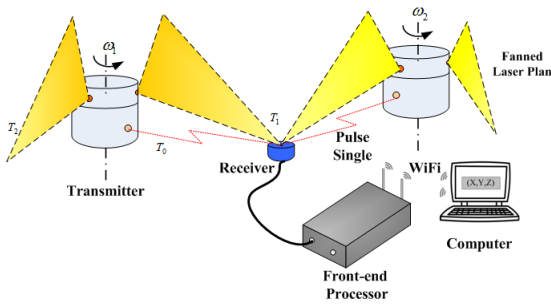The mathematical model is based on two important coordinate systems which are defined as follows (Fig. 2 and Fig. 3).
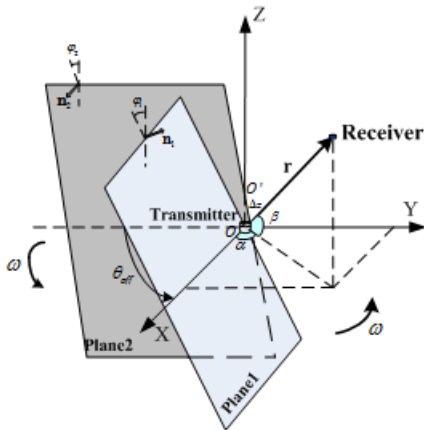
FIGURE 1. A directed acyclic graph.

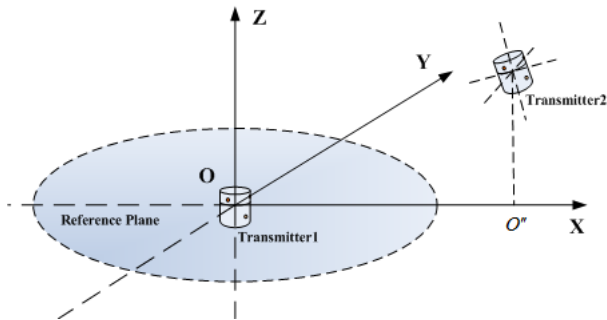**FIGURE 2.** A directed acyclic graph.

FIGURE 3. A directed acyclic graph.

Transmitter coordinate system (marked as *t*): Z-axis is the transmitter's rotation axis which two laser planes rotate around. Origin is the intersection of laser plane **1** and Z-axis. X-axis is the intersecting line between the laser plane **1** and the vertical plane of Z-axis when the laser plane **1** rotates to the starting time (T_0). Y-axis is determined according to the right-hand rule.

Global coordinate system (marked as *g*): The coordinate system is based on two transmitters. Its Z-axis and Origin are the Z-axis and Origin of transmitter **1**'s coordinate system respectively. Supposing that the projection point of transmitter **2** on the vertical plane of Z-axis is O'', then X-axis is the connection between the Origin and O''. Also Y-axis is determined according to the right-hand rule.

The transformation relation between the two coordinate systems can be described as:

$$\begin{bmatrix} x_g \\ y_g \\ z_g \end{bmatrix} = R \begin{bmatrix} x_t \\ y_t \\ z_t \end{bmatrix} + V \tag{2}$$

where R is the rotation matrix which can be represented by three Euler angles, V is the translation matrix which consists of the transmitter's coordinates in global coordinate system. We define R and V as external parameters and these external parameters can be determined by calibrating [24].

Besides, there are some basic parameters in the transmitter coordinate system. According to Fig. 2 and Fig. 3, φ_1 and φ_2 are the inclined angles of laser Plane**1** and laser Plane**2**, and θ_{off} is a fixed offset angle between the two laser planes. Since two laser plans and the Z-axis cannot intersect at one point (the Origin) in the transmitter coordinate system because of the assembly error, we suppose the laser Plane**2** intersects the Z-axis at O', then Δz is defined as the distance between the Origin and the O'. These parameters ($\varphi_1, \varphi_2, \theta_{off}$, and Δz) can be regarded as internal parameters, because they only depend on the assembly process, and they can be treated as constants as soon as the transmitter is completed.

Based on the coordinate systems and external/internal parameters defined above, the 3D coordinates can be calculated according to the bundle adjustment based on the photogrammetry. The method is described in detail as below.

When the laser plane **1** rotates to the starting time T_0, the normal vectors of the two planes can be expressed as Equation (3) and Equation (4) in transmitter coordinate system:

$$\pmb{n}_1^0 = \begin{bmatrix} 1 & 0 & 0 \\ 0 & \cos \varphi_1 & -\sin \varphi_1 \\ 0 & \sin \varphi_1 & \cos \varphi_1 \end{bmatrix} \begin{bmatrix} 0 \\ 1 \\ 0 \end{bmatrix} = \begin{bmatrix} 0 \\ \cos \varphi_1 \\ \sin \varphi_1 \end{bmatrix} \tag{3}$$

$$\pmb{n}_2^0 = \begin{bmatrix} \cos \theta_{off} & -\sin \theta_{off} & 0 \\ \theta_{off} & \cos \theta_{off} & 0 \\ 0 & 0 & 1 \end{bmatrix} \begin{bmatrix} 0 \\ \cos \varphi_2 \\ \sin \varphi_2 \end{bmatrix}$$

$$= \begin{bmatrix} -\sin \theta_{off} \cos \varphi_2 \\ \cos \theta_{off} \cos \varphi_2 \\ \sin \varphi_2 \end{bmatrix} \tag{4}$$

When the two laser planes sweep over the receiver at time T_1 and T_2 in turn, the normal vectors change into:

$$\pmb{n}_1^T = \begin{bmatrix} \cos \theta_1 & -\sin \theta_1 & 0 \\ \sin \theta_1 & \cos \theta_1 & 0 \\ 0 & 0 & 1 \end{bmatrix} \pmb{n}_1^0 = \begin{bmatrix} -\sin \theta_1 \cos \varphi_1 \\ \cos \theta_1 \cos \varphi_1 \\ \sin \varphi_1 \end{bmatrix} \tag{5}$$

$$\pmb{n}_2^T = \begin{bmatrix} \cos \theta_2 & -\sin \theta_2 & 0 \\ \sin \theta_2 & \cos \theta_2 & 0 \\ 0 & 0 & 1 \end{bmatrix} \pmb{n}_2^0$$

$$= \begin{bmatrix} -\sin (\theta_2 + \theta_{off}) \cos \varphi_2 \\ \cos (\theta_2 + \theta_{off}) \cos \varphi_2 \\ \sin \varphi_2 \end{bmatrix} \tag{6}$$

where θ_1 and θ_2 can be obtained by Equation(1).

According to the bundle adjustment algorithm, the plane parameter equation in transmitter coordinate system can be written as Equation(7).

$$\begin{cases} a_1^t x_t^r + b_1^t y_t^r + c_1^t z_t^r + d_1^t = 0 \\ a_2^t x_t^r + b_2^t y_t^r + c_2^t z_t^r + d_2^t = 0 \end{cases} \tag{7}$$

where $\left[a_1^t, b_1^t, c_1^t, d_1^t\right]^T$ and $\left[a_2^t, b_2^t, c_2^t, d_2^t\right]^T$ are the two laser planes' parameters in the transmitter coordinate system when the laser plane sweep over the receiver, respectively, and they can be defined as follows based on Equation(5) and Equation(6). $X_t^r \left(x_t^r, y_t^r, z_t^r\right)$ is the receiver coordinates in the transmitter coordinate system.

$$\begin{bmatrix} a_1^t \\ b_1^t \\ c_1^t \\ d_1^t \end{bmatrix} = \begin{bmatrix} -\sin\theta_1 \cos\varphi_1 \\ \cos\theta_1 \cos\varphi_1 \\ \sin\varphi_1 \\ 0 \end{bmatrix} \tag{8}$$

$$\begin{bmatrix} a_2^t \\ b_2^t \\ c_2^t \\ d_2^t \end{bmatrix} = \begin{bmatrix} -\sin\left(\theta_2 + \theta_{off}\right) \cos\varphi_2 \\ \cos\left(\theta_2 + \theta_{off}\right) \cos\varphi_2 \\ \sin\varphi_2 \\ -\Delta z \cdot \sin\varphi_2 \end{bmatrix} \tag{9}$$

To calculate the receiver coordinates in the global coordinate system $X_g^r \left(x_g^r, y_g^r, z_g^r\right)$, according to Equation (2), transforming $\left[a_1^t, b_1^t, c_1^t, d_1^t\right]^T$ and $\left[a_2^t, b_2^t, c_2^t, d_2^t\right]^T$ into the global coordinate system.

$$\begin{bmatrix} a_1^g \\ b_1^g \\ c_1^g \\ d_1^g \end{bmatrix} = \begin{bmatrix} \begin{bmatrix} R & V \\ 0 & 1 \end{bmatrix}^{-1} \end{bmatrix}^T \begin{bmatrix} a_1^t \\ b_1^t \\ c_1^t \\ d_1^t \end{bmatrix} \tag{10}$$

$$\begin{bmatrix} a_2^g \\ b_2^g \\ c_2^g \\ d_2^g \end{bmatrix} = \begin{bmatrix} \begin{bmatrix} R & V \\ 0 & 1 \end{bmatrix}^{-1} \end{bmatrix}^T \begin{bmatrix} a_2^t \\ b_2^t \\ c_2^t \\ d_2^t \end{bmatrix} \tag{11}$$

where $\left[a_1^g, b_1^g, c_1^g, d_1^g\right]^T$ and $\left[a_2^g, b_2^g, c_2^g, d_2^g\right]^T$ are the two laser planes' parameters of transmitter in the global coordinate system.

If there are at least two transmitters sweep over the receiver, the receiver coordinates $X_g^r \left(x_g^r, y_g^r, z_g^r\right)$ can be calculated using the following formulas.

$$\begin{cases} a_{11}^g x_g^r + b_{11}^g y_g^r + c_{11}^g z_g^r + d_{11}^g = 0 \\ a_{12}^g x_g^r + b_{12}^g y_g^r + c_{12}^g z_g^r + d_{12}^g = 0 \\ \vdots \\ a_{n1}^g x_g^r + b_{n1}^g y_g^r + c_{n1}^g z_g^r + d_{n1}^g = 0 \\ a_{n2}^g x_g^r + b_{n2}^g y_g^r + c_{n2}^g z_g^r + d_{n2}^g = 0 \end{cases} \tag{12}$$

The symbol n is the number of transmitters.

Equation (12) can be arranged in the following form if $n \geq 2$:

$$AX_g^r = B \tag{13}$$

Since Equation (13) is an over-determined equation, thus the optimal solution of receiver coordinates X_g^r can be calculated based on LSE as shown in Equation (14).

$$X_g^r = \left(A^T A\right)^{-1} A^T B \tag{14}$$

According to Equation (14), we can know that the condition for the coordinate calculating is that the receiver should receive signals from at least two transmitters. Therefore, during positioning, no matter the number of transmitters increases or decreases, as long as the number of working transmitters is not less than two, the system can work normally.

Section 1 has analyzed the strength and weakness of the above solution mathematical model in-depth. In order to further optimize the coordinate positioning algorithm, we start to study the factor graph and sum-product algorithm in the next section.

III. 3D COORDINATE POSITIONING ALGORITHM BASED ON FG
A. FACTOR GRAPH AND SUM-PRODUCT ALGORITHM
Factor graph is a probabilistic graph model based on Bayesian network, which transforms the global function into the product of nodes function by factor decomposition [25]–[27]. Thus it has the characteristic of visualizing the complex variable relations. The FG is composed of variable nodes and function nodes. The variable nodes are connected with the corresponding function nodes by the edge line to realize the information transmission between them, and we define the information as soft information (SI). Due to the bidirectional nature of information, SI can be divided into two types, namely, information passed from the variable node to the function node and information passed from the function node to the variable node. SI is often calculated by the sum-product algorithm, and the algorithm's basic principle is that the SI passed from the variable node to the measured function node is equal to the product of all the function nodes' SI passed to the variable node except the measured function node' SI.

Fig. 4 shows a typical FG model. In this model, x stands for the variable node; f stands for the function node; H stands for the set of all function nodes connected to x; H/f stands for the set of all function nodes connected to x except function node f; Similarly, Y stands for the set of all variable nodes connected to f; Y/x stands for the set of all variable nodes connected to f except variable node x. $\mu_{x \to f}(x)$ stands for the SI passed from the variable node x to the function node f; $\mu_{f \to x}(x)$ stands for the SI passed from the function node f to the variable node x; Similarly, $\mu_{y_1 \to f}(y_1)$ stands for the SI passed from the variable node y_1 to the function node f; stands for the SI passed from the function node h_1 to the variable node x. $\mu_{x \to f}(x)$ and $\mu_{f \to x}(x)$ is calculated as Equation (15). Where $\sim x$ is the variable nodes connected with
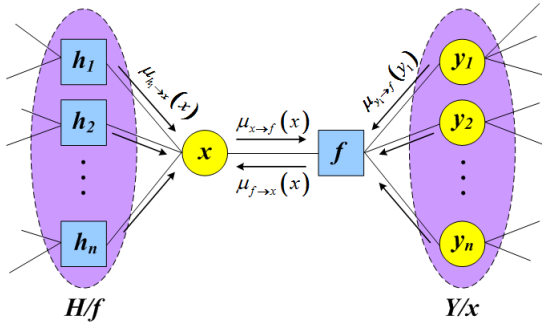
FIGURE 4. A directed acyclic graph.

FIGURE 5. A directed acyclic graph.

the function node f except the variable node x.

$$\begin{cases} \mu_{x \to f}(x) = \prod_{H/f} \mu_{h \to x}(x) \\ \mu_{f \to x}(x) = \sum_{\sim x} \left\{ f(Y) \prod_{Y/x} \mu_{y \to f}(y) \right\} \end{cases} \quad (15)$$

B. 3D COORDINATE POSITIONING METHOD BASED ON FG

1) MATHEMATICAL MODEL

According to the characteristics of information transmission in iGPS and wMPS, a mathematical model based on distributed FG is constructed, as shown in Fig. 5. Supposing the positioning coordinate of the measured point at Time $k-1$ is $F_{k-1} = \{x_{k-1}, y_{k-1}, z_{k-1}\}$, and the estimated coordinate at Time k is $F_k = \{x_k, y_k, z_k\}$. Due to the information transmission in this system is real-time, the transmission of SI is set to one-way delivery mode. Take the X-direction as an example, x_k^0 is the initial coordinate node, $x_k^1, x_k^2, \cdots, x_k^n$ stands for the state nodes after updating, ω_{x_k} stands for the noise, $\theta_k^1, \theta_k^2, \cdots, \theta_k^{n-1}$ stands for the measurement information nodes from different transmitter, $\tilde{x}_k^1, \tilde{x}_k^2, \cdots, \tilde{x}_k^n$ stands for the updated state nodes according to the measurement information, $h_{\theta x_k^1}, h_{\theta x_k^2}, \cdots, h_{\theta x_k^{n-1}}$ stands for the measurement node functions, and $f_w, f_{x_k^1}, f_{x_k^2}, \cdots, f_{x_k^{n-1}}$ stands for the update node functions. Based on the thought of maximum posteriori estimation criterion, the functions update the state information at first and then the measurement information. Through calculating a series of SI, the positioning result x_k^n is obtained. Similarly, the positioning result in the Y-direction and the Z-direction are obtained. Thus the positioning coordinate at Time k is $F_k = \{x_k^n, y_k^n, z_k^n\}$.

As shown in Fig. 5, due to the plug-and-play characteristics of FG, the FG algorithm takes the transmitters' information (θ_k^n) as measurement information and the algorithm is calculated sequentially using the measurement information. The number change of transmitters only influences the number of iterations. For example, if there are 3 transmitters in the system at first, this means there are 3 measurement information, and then the position result can be output after 3 times iterative update. If one of the transmitters fails at Time k, then
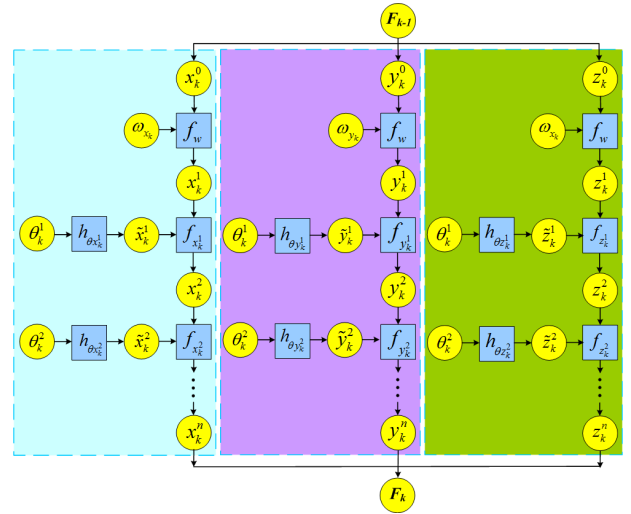
the position result is output with 2 times' iterative update at Time k. The system still works. However, as for the traditional LSE algorithm, according to Equation (14), for different number of transmitters, the mathematical model is different. This will cause a problem that once the transmitters' number changes, the LSE algorithm will take one cycle to determine the number of transmitters and reselect the mathematical model to position. Thus if the transmitters' number changes from 3 to 2 at Time k, then the LSE algorithm will not output the positioning result at Time k. Similarly, if the transmitters' number increases at Time k, the iterations number of FG algorithm increases correspondingly, and the results can be output at Time k, while LSE will not be output the results at Time k due to the changes in the mathematical model.

According to Fig. 5, observations from different transmitters are unrelated with each other. From the perspective of statistics, the error of independent observation information is also random, and this error will be brought into the positioning results. For example, if the observation information has a large gross error at a certain time, the positioning results will also contain a large outlier and we can't handle it, resulting in a decrease in the confidence of the positioning results. At the same time, independent observation information can only affect the positioning result of a certain moment. If the observation information of a certain moment is particularly good, it can only obtain good positioning information at that moment, but fails to improve the positioning accuracy of the subsequent moments, resulting in a waste of observation information resources. So, in order to avoid these problems, reduce the influence of the random error, and improve the effect of good observation information, the proposed FG algorithm using the ideas of iteration, through using the positioning result at Time k-1 and observation information at Time k, obtains the positioning result at Time k. This process can be regarded as link all independent observation information and make the results relevant.

2) THE CALCULATION METHOD OF SI

We still take the X-direction as an example. At first, let's calculate the SI passed from the variable node θ_k^{n-1} to the function node $h_{\theta x_k^{n-1}}$, shown as Equation(16).

$$\mu_{\theta \to h}\left(\theta_k^{n-1}\right) = \theta_k^{n-1} \tag{16}$$

Supposing θ_k^{n-1} satisfies the Gaussian distribution of expectation $m_{\theta_k^{n-1}}$ and variance $\sigma_{\theta_k^{n-1}}^2$, namely, $\theta_k^{n-1} \sim N\left(\theta_k^{n-1}, m_{\theta_k^{n-1}}, \sigma_{\theta_k^{n-1}}^2\right)$. So the SI in Equation (16) can be written as Equation (17).

$$SI = \left\{ m_{\theta_k^{n-1}}, \sigma_{\theta_k^{n-1}}^2 \right\} \tag{17}$$

Then let's calculate the SI passed from the function node $h_{\theta x_k^{n-1}}$ to the variable node $\tilde{x}_k^{n-1}$. According to Equation (7)-Equation (11), since there are two plane parameter equations, so $\mu_{h_\theta \to \tilde{x}_k^{n-1}}$ can be calculated as two forms.

$$
\begin{aligned}
& \mu_{h_\theta \to \tilde{x}_k^{n-1}} \\
& = [c_{10} \cos\varphi \sin\theta_{x_k^{n-1}} - c_{11} \cos\varphi \cos\theta_{x_k^{n-1}} - c_{12}\sin\varphi \\
& \quad - y(-c_4 \sin\varphi \sin\theta_{x_k^{n-1}} + c_5 \cos\varphi \cos\theta_{x_k^{n-1}} + c_6\sin\varphi) \\
& \quad - z(-c_7 \cos\varphi \sin\theta_{x_k^{n-1}} + c_8 \cos\varphi \cos\theta_{x_k^{n-1}} + c_9\sin\varphi)] \\
& \quad /(-c_1 \cos\varphi \sin\theta_{x_k^{n-1}} + c_2 \cos\varphi \cos\theta_{x_k^{n-1}} + c_3\sin\varphi)
\end{aligned} \tag{18}
$$

Or

$$
\begin{aligned}
& \mu_{h_\theta \to \tilde{x}_k^{n-1}} \\
& = \{c_{10} \cos\varphi \sin(\theta_{x_k^{n-1}} + \theta_{off}) - c_{11} \cos\varphi \cos(\theta_{x_k^{n-1}} \\
& \quad + \theta_{off}) - c_{12}\sin\varphi + \Delta z \sin\varphi_2 - y[-c_4 \sin\varphi \sin(\theta_{x_k^{n-1}} \\
& \quad + \theta_{off}) + c_5 \cos\varphi \cos(\theta_{x_k^{n-1}} + \theta_{off}) + c_6\sin\varphi] \\
& \quad - z[-c_7 \cos\varphi \sin(\theta_{x_k^{n-1}} + \theta_{off}) + c_8 \cos\varphi \cos(\theta_{x_k^{n-1}} \\
& \quad + \theta_{off}) + c_9\sin\varphi]\}/[-c_1 \cos\varphi \sin(\theta_{x_k^{n-1}} + \theta_{off}) \\
& \quad + c_2 \cos\varphi \cos(\theta_{x_k^{n-1}} + \theta_{off}) + c_3\sin\varphi]
\end{aligned} \tag{19}
$$

where

$$
\begin{bmatrix} c_1 & c_2 & c_3 & 0 \\ c_4 & c_5 & c_6 & 0 \\ c_7 & c_8 & c_9 & 0 \\ c_{10} & c_{11} & c_{12} & 1 \end{bmatrix} = \left[\begin{bmatrix} \boldsymbol{R} & \boldsymbol{V} \\ \boldsymbol{0} & 1 \end{bmatrix}^{-1} \right]^T .
$$

Since we know $\theta_k^{n-1} \sim N\left(\theta_k^{n-1}, m_{\theta_k^{n-1}}, \sigma_{\theta_k^{n-1}}^2\right)$, thus we can calculate the expectation and variance of $\tilde{x}_k^{n-1}$ according to Equation (18) and Equation (19).

If the function $Y = \mu_{h_\theta \to \tilde{x}_k^{n-1}}(\theta)$ has a first-order derivative in the neighborhood of $\theta = \theta_k^{n-1}$, then let's expand to the first-order Taylor equation at $\theta = \theta_k^{n-1}$ [28].

$$
\begin{aligned}
Y &= \mu_{h_\theta \to \tilde{x}_k^{n-1}}(\theta) \\
&\approx \mu_{h_\theta \to \tilde{x}_k^{n-1}}\left(\theta_k^{n-1}\right) + \mu'_{h_\theta \to \tilde{x}_k^{n-1}}\left(\theta - \theta_k^{n-1}\right)
\end{aligned} \tag{20}
$$

So the expectation can be express as:

$$
\begin{aligned}
& m_{\tilde{x}_k^{n-1}} \\
& = E(Y) \\
& \approx E\left[\mu_{h_\theta \to \tilde{x}_k^{n-1}}\left(\theta_k^{n-1}\right) + \mu'_{h_\theta \to \tilde{x}_k^{n-1}}\left(\theta - \theta_k^{n-1}\right)\right] \\
& = E\left[\mu_{h_\theta \to \tilde{x}_k^{n-1}}\left(\theta_k^{n-1}\right)\right] + E\left[\mu'_{h_\theta \to \tilde{x}_k^{n-1}}\left(\theta - \theta_k^{n-1}\right)\right] \\
& = E\left[\mu_{h_\theta \to \tilde{x}_k^{n-1}}\left(\theta_k^{n-1}\right)\right] + \mu'_{h_\theta \to \tilde{x}_k^{n-1}} E\left(\theta - \theta_k^{n-1}\right) \\
& = \mu_{h_\theta \to \tilde{x}_k^{n-1}}\left(m_{\theta_k^{n-1}}\right)
\end{aligned} \tag{21}
$$

And the variance can be express as:

$$
\begin{aligned}
& \sigma_{\tilde{x}_k^{n-1}}^2 = D(Y) \\
& \approx D\left[\mu_{h_\theta \to \tilde{x}_k^{n-1}}\left(\theta_k^{n-1}\right) + \mu'_{h_\theta \to \tilde{x}_k^{n-1}}\left(\theta - \theta_k^{n-1}\right)\right] \\
& = D\left[\mu_{h_\theta \to \tilde{x}_k^{n-1}}\left(\theta_k^{n-1}\right)\right] + D\left[\mu'_{h_\theta \to \tilde{x}_k^{n-1}}\left(\theta - \theta_k^{n-1}\right)\right] \\
& = \mu'_{h_\theta \to \tilde{x}_k^{n-1}} D\left(\theta - \theta_k^{n-1}\right) = \mu'_{h_\theta \to \tilde{x}_k^{n-1}} \sigma_{\theta_k^{n-1}}^2
\end{aligned} \tag{22}
$$

From the above, $\tilde{x}_k^{n-1} \sim N\left(\tilde{x}_k^{n-1}, m_{\tilde{x}_k^{n-1}}, \sigma_{\tilde{x}_k^{n-1}}^2\right)$. So the SI in Equation (18) and Equation (19) can be written as Equation (23).

$$SI = \left\{ m_{\tilde{x}_k^{n-1}}, \sigma_{\tilde{x}_k^{n-1}}^2 \right\} \tag{23}$$

At last, the SI passed from the function node $f_{x_k^{n-1}}$ to the variable node x_k^n can be obtained, shown as Equation (24).

$$\mu_{f_{x_k^{n-1}} \to x_k^n} = f_{x_k^{n-1}} \mu_{\tilde{x}_k^{n-1} \to f_{x_k^{n-1}}} \mu_{x_k^{n-1} \to f_{x_k^{n-1}}} \tag{24}$$

The update node function $f_{x_k^{n-1}} = 1$.

Since the product of functions which satisfy the Gaussian probability distribution still satisfies the Gaussian distribution, the state node x_k^n can be represented by Equation (25).

$$\prod_{i=1}^{n} N\left(x, m_i, \sigma_i^2\right) \propto N\left(x_k^n, m_{x_k^n}, \sigma_{x_k^n}^2\right) \tag{25}$$

During updating, the transformation relation about expectation and variance are shown in Equation (26).

$$
\begin{cases}
\dfrac{1}{\sigma_{x_k^n}^2} = \displaystyle\sum_{i=1}^{n} \dfrac{1}{\sigma_i^2} \\
m_{x_k^n} = \sigma_{x_k^n}^2 \displaystyle\sum_{i=1}^{n} \dfrac{m_i}{\sigma_i^2}
\end{cases} \tag{26}
$$

According to Fig. 5, we suppose that the initial coordinate node $x_k^0 \sim N\left(x_k^0, m_{x_k^0}, \sigma_{x_k^0}^2\right)$, which can be gotten by LSE, and its noise $\omega_k \sim \left(\omega_k, m_{\omega_k}, \sigma_{\omega_k}^2\right)$, thus the SI passed from

the function node f to the variable node x_k^n can be shown as Equation (27).

$$
\begin{cases}
SI_{x_k^1} = \left\{ m_{x_k^0} + m_{\omega_k}, \sigma_{x_k^0}^2 + \sigma_{\omega_k}^2 \right\} \\[2mm]
SI_{x_k^2} = \left\{ \dfrac{1}{1 \big/ \sigma_{x_k^1}^2 + 1 \big/ \sigma_{\tilde{x}_k^1}^2} \left(\dfrac{m_{x_k^1}}{\sigma_{x_k^1}^2} + \dfrac{m_{\tilde{x}_k^1}}{\sigma_{\tilde{x}_k^1}^2} \right), \dfrac{1}{1 \big/ \sigma_{x_k^1}^2 + 1 \big/ \sigma_{\tilde{x}_k^1}^2} \right\} \\[3mm]
SI_{x_k^3} = \left\{ \dfrac{1}{1 \big/ \sigma_{x_k^2}^2 + 1 \big/ \sigma_{\tilde{x}_k^2}^2} \left(\dfrac{m_{x_k^2}}{\sigma_{x_k^2}^2} + \dfrac{m_{\tilde{x}_k^2}}{\sigma_{\tilde{x}_k^2}^2} \right), \dfrac{1}{1 \big/ \sigma_{x_k^2}^2 + 1 \big/ \sigma_{\tilde{x}_k^2}^2} \right\} \\[2mm]
\qquad\qquad\qquad \vdots \\[2mm]
SI_{x_k^n} = \left\{ \dfrac{1}{1 \big/ \sigma_{x_k^{n-1}}^2 + 1 \big/ \sigma_{\tilde{x}_k^{n-1}}^2} \left(\dfrac{m_{x_k^{n-1}}}{\sigma_{x_k^{n-1}}^2} + \dfrac{m_{\tilde{x}_k^{n-1}}}{\sigma_{\tilde{x}_k^{n-1}}^2} \right), \right. \\[3mm]
\qquad\qquad \left. \dfrac{1}{1 \big/ \sigma_{x_k^{n-1}}^2 + 1 \big/ \sigma_{\tilde{x}_k^{n-1}}^2} \right\}
\end{cases}
\tag{27}
$$

$m_{x_k^n}$ is the final updated expectation in X-direction, let $x_k^n = m_{x_k^n}$, namely, the positioning coordinate in X-direction at Time k is shown as Equation (28).

$$
x_k^n = \frac{1}{1 \big/ \sigma_{x_k^{n-1}}^2 + 1 \big/ \sigma_{\tilde{x}_k^{n-1}}^2} \left(\frac{m_{x_k^{n-1}}}{\sigma_{x_k^{n-1}}^2} + \frac{m_{\tilde{x}_k^{n-1}}}{\sigma_{\tilde{x}_k^{n-1}}^2} \right)
\tag{28}
$$

Similarly, the positioning coordinate y_k^n, z_k^n in Y-direction and Z-direction at Time k is shown as Equation (29).

$$
\begin{cases}
y_k^n = \dfrac{1}{1 \big/ \sigma_{y_k^{n-1}}^2 + 1 \big/ \sigma_{\tilde{y}_k^{n-1}}^2} \left(\dfrac{m_{y_k^{n-1}}}{\sigma_{y_k^{n-1}}^2} + \dfrac{m_{\tilde{y}_k^{n-1}}}{\sigma_{\tilde{y}_k^{n-1}}^2} \right) \\[4mm]
z_k^n = \dfrac{1}{1 \big/ \sigma_{z_k^{n-1}}^2 + 1 \big/ \sigma_{\tilde{z}_k^{n-1}}^2} \left(\dfrac{m_{z_k^{n-1}}}{\sigma_{z_k^{n-1}}^2} + \dfrac{m_{\tilde{z}_k^{n-1}}}{\sigma_{\tilde{z}_k^{n-1}}^2} \right)
\end{cases}
\tag{29}
$$

From Equation (27) - Equation (29), we can see that the update of the status node is related to the measurement information and the previous status node information, which reduces the independence of the positioning results. Thus the positioning results can be output optimally.

3) ALGORITHM PERFORMANCE ANALYSIS

In order to analyze the effectiveness of the proposed algorithm in theory, taking X-direction as an example, we study the relationship among the status update node $\tilde{x}_k$ obtained by the measurement information, the previous status update node x_{k-1} and the status update node x_k based on the FG, and the three SI are shown as Equation (30).

$$
\begin{cases}
SI_{\tilde{x}_k} = \left\{ m_{\tilde{x}_k}, \sigma_{\tilde{x}_k}^2 \right\} \\
SI_{x_{k-1}} = \left\{ m_{x_{k-1}}, \sigma_{x_{k-1}}^2 \right\} \\
SI_{x_k} = \left\{ m_{x_k}, \sigma_{x_k}^2 \right\}
\end{cases}
\tag{30}
$$

According to the principle of positioning algorithm based on FG, the relationship among the three SI can be written as follows.

$$
\begin{cases}
\sigma_{x_k}^2 = \dfrac{1}{1 \big/ \sigma_{\tilde{x}_k}^2 + 1 \big/ \sigma_{x_{k-1}}^2} \\[4mm]
m_{x_k} = \sigma_{x_k}^2 \left(\dfrac{m_{\tilde{x}_k}}{\sigma_{\tilde{x}_k}^2} + \dfrac{m_{x_{k-1}}}{\sigma_{x_{k-1}}^2} \right)
\end{cases}
\tag{31}
$$

At first, comparing the variance of $\tilde{x}_k$, x_{k-1} and x_k. Arranging $\sigma_{x_k}^2$ as Equation (32).

$$
\begin{aligned}
\sigma_{x_k}^2 &= \frac{\sigma_{\tilde{x}_k}^2 \sigma_{x_{k-1}}^2}{\sigma_{\tilde{x}_k}^2 + \sigma_{x_{k-1}}^2} = \frac{\sigma_{\tilde{x}_k}^2}{\sigma_{\tilde{x}_k}^2 + \sigma_{x_{k-1}}^2} \sigma_{x_{k-1}}^2 \\
&= \frac{\sigma_{x_{k-1}}^2}{\sigma_{\tilde{x}_k}^2 + \sigma_{x_{k-1}}^2} \sigma_{\tilde{x}_k}^2
\end{aligned}
\tag{32}
$$

Since $\frac{\sigma_{\tilde{x}_k}^2}{\sigma_{\tilde{x}_k}^2 + \sigma_{x_{k-1}}^2} < 1$, $\frac{\sigma_{x_{k-1}}^2}{\sigma_{\tilde{x}_k}^2 + \sigma_{x_{k-1}}^2} < 1$, so we have:

$$
\begin{cases}
\sigma_{x_k}^2 < \sigma_{x_{k-1}}^2 \\
\sigma_{x_k}^2 < \sigma_{\tilde{x}_k}^2
\end{cases}
\tag{33}
$$

According to Equation (33), the fusion variance based on FG is smaller than the variance of the two kinds of fusion sources. Since $\sigma_{x_k}^2 < \sigma_{\tilde{x}_k}^2$, the algorithm based on FG is convergent, thus the positioning results will gradually close to the true value with the increase of the number of iterations.

Then comparing the expectation of $\tilde{x}_k$, x_{k-1} and x_k. Supposing the real positioning is $m_{x_k}^r$, so the errors of the three status nodes $\varepsilon_{\tilde{x}_k}$, $\varepsilon_{x_{k-1}}$ and ε_{x_k} can be confirmed as follows.

$$
\begin{cases}
\varepsilon_{\tilde{x}_k} = \left| m_{\tilde{x}_k} - m_{x_k}^r \right| \\
\varepsilon_{x_{k-1}} = \left| m_{x_{k-1}} - m_{x_k}^r \right| \\
\varepsilon_{x_k} = \left| m_{x_k} - m_{x_k}^r \right|
\end{cases}
\tag{34}
$$

Discussing the relationship of $\varepsilon_{\tilde{x}_k}$ and ε_{x_k} by making a difference shown as follows.

$$
\varepsilon = \varepsilon_{x_k}^2 - \varepsilon_{\tilde{x}_k}^2 = \left(m_{x_k} - m_{x_k}^r \right)^2 - \left(m_{\tilde{x}_k} - m_{x_k}^r \right)^2
\tag{35}
$$

So the comparison of $\tilde{x}_k$ and x_k turns into the comparison of ε and 0. Since $m_{x_k}^r$ is a constant, to simplify the calculation, let $m_{x_k}^r = 0$, thus Equation (35) can be expressed as Equation (36).

$$
\varepsilon = m_{x_k}^2 - m_{\tilde{x}_k}^2
\tag{36}
$$

Plugging Equation (32) into Equation (36), we have:

$$
\begin{aligned}
\varepsilon &= \left[\frac{1}{1 \big/ \sigma_{\tilde{x}_k}^2 + 1 \big/ \sigma_{x_{k-1}}^2} \left(\frac{m_{\tilde{x}_k}}{\sigma_{\tilde{x}_k}^2} + \frac{m_{x_{k-1}}}{\sigma_{x_{k-1}}^2} \right) \right]^2 - m_{\tilde{x}_k}^2 \\
&= \left(\frac{\sigma_{\tilde{x}_k}^2}{\sigma_{\tilde{x}_k}^2 + \sigma_{x_{k-1}}^2} m_{x_{k-1}} + \frac{\sigma_{x_{k-1}}^2}{\sigma_{\tilde{x}_k}^2 + \sigma_{x_{k-1}}^2} m_{\tilde{x}_k} \right)^2 - m_{\tilde{x}_k}^2
\end{aligned}
\tag{37}
$$

Let $a = \frac{\sigma_{\tilde{x}_k}^2}{\sigma_{\tilde{x}_k}^2 + \sigma_{x_{k-1}}^2}$, so we have $\frac{\sigma_{x_{k-1}}^2}{\sigma_{\tilde{x}_k}^2 + \sigma_{x_{k-1}}^2} = 1-a$, and $0 < a < 1$. Rewrite Equation (37) as follows.

$$\varepsilon = \left[am_{x_{k-1}} + (1-a)m_{\tilde{x}_k}\right]^2 - m_{\tilde{x}_k}^2$$
$$= a^2 m_{x_{k-1}}^2 + 2a(1-a)m_{x_{k-1}}m_{\tilde{x}_k} + \left(a^2 - 2a\right)m_{\tilde{x}_k}^2 \quad (38)$$

Equation (38) is a quadratic equation of one variable about $m_{\tilde{x}_k}$, and $\left(a^2 - 2a\right) < 0$. So if we want $\varepsilon < 0$, we just need $m_{\tilde{x}_k} < x_1$ or $m_{\tilde{x}_k} > x_2$, x_1, x_2 are shown as Equation (39).

$$\begin{cases} x_1 = \dfrac{am_{x_{k-1}}}{a-2} \\ x_2 = m_{x_{k-1}} \end{cases} \quad (39)$$

Supposing $m_{x_k} > 0, m_{x_{k-1}} > 0$, $m_{\tilde{x}_k} > 0$, thus $m_{x_k} < m_{\tilde{x}_k}$ as long as $m_{x_{k-1}} < m_{\tilde{x}_k}$. Similarly, $m_{x_k} < m_{x_{k-1}}$ as long as $m_{\tilde{x}_k} < m_{x_{k-1}}$. In summary, $\min\left(m_{x_{k-1}}, m_{\tilde{x}_k}\right) < m_{x_k} < \max\left(m_{x_{k-1}}, m_{\tilde{x}_k}\right)$. This means the expectation m_{x_k} is bounded and will converge to truth gradually.

Moreover, writing Equation (31) as follows:

$$\begin{cases} \sigma_{x_k}^2 = \dfrac{\sigma_{\tilde{x}_k}^2 \sigma_{x_{k-1}}^2}{\sigma_{\tilde{x}_k}^2 + \sigma_{x_{k-1}}^2} \\ m_{x_k} = \dfrac{\sigma_{\tilde{x}_k}^2 m_{x_{k-1}} + \sigma_{x_{k-1}}^2 m_{\tilde{x}_k}}{\sigma_{\tilde{x}_k}^2 + \sigma_{x_{k-1}}^2} \end{cases} \quad (40)$$

Since the variance $\sigma_{x_{k-1}}^2$ is convergent, which means $\sigma_{x_{k-1}}^2$ will be a small quantity after several iterations, so if there is a gross error in $m_{\tilde{x}_k}$, it won't cause a big interference for the result because of the tiny weight. And when the measurement expectation $m_{\tilde{x}_k}$ is gradually close to the real expectation, its measurement variance $\sigma_{\tilde{x}_k}^2$ will also become small. In this way, when the measurement expectation $m_{\tilde{x}_k}$ is better than the estimated expectation $m_{x_{k-1}}$, its variance $\sigma_{\tilde{x}_k}^2$ will be better than the estimated variance $\sigma_{x_{k-1}}^2$, and the updated result m_{x_k} will be closer to the measurement expectation $m_{x_{k-1}}$, as a result, the positioning result will be further optimized.

According to the above analysis, when there is a gross measurement error in the update process, the algorithm based on the FG can reduce the impact of the gross error to a great extent and improve the robustness and stability of the system; and when the measurement information performs well, the system positioning result become closer to the real value. To sum up, the proposed algorithm based on FG is very robust in theory.

IV. RESULTS

To verify the effect of proposed algorithm based on FG, a series of simulations and prototype tests have been designed and carried out.

A. SIMULATION EXPERIMENT

The simulation environment is built at first. According to the coordinate system definition in Section 2, in order to simulate the system, we suppose that the system has been calibrated, and the relative relationship between the transmitter coordinate system and the global coordinate system are directly given, namely, we think the transmitters' external parameters and internal parameters are known. Meantime the receivers' true coordinates in the global coordinate system are also known as the true value, so the true scanning angles θ_1, θ_2 of the transmitter sweeping over the receiver can be calculated. According to [29], the external errors can be uniformly converted into the scanning angle error, so the random scanning angle errors $\Delta\theta_1, \Delta\theta_2$ are added into the obtained scanning angles to simulate the actual working state of this system. Based on the scanning angles with errors, the proposed positioning algorithm based on FG can be tested.

1) SINGLE-POINT POSITIONING EXPERIMENT

The experimental conditions of single-point positioning are shown in Table 1. To simulate the plug-and-play nature of this system, a three-transmitters positioning scheme has been used at first. The three transmitters are called T_1, T_2, and T_3 for short, and T_3 has been removed for a period of time during the experiment. For the convenience of analysis, the same parameter information has been used in the three transmitters, and the scanning angle errors of the transmitters also be set at a same level. We have carried 100 times positioning simulation experiment. To compare the performance of the algorithms based on FG and LSE, the two algorithms are both simulated, and the results are shown as Fig.6 to Fig. 9. The positioning error $\Delta R(\Delta X, \Delta Y, \Delta Z)$ in different axes is obtained by Equation (41), and the total positioning error Δd is obtained by Equation (42).

$$\Delta R = R_{true} - R_{calculate} \quad (41)$$
$$\Delta d = \sqrt{\Delta X^2 + \Delta Y^2 + \Delta Z^2} \quad (42)$$

TABLE 1. The experimental conditions of single-point positioning.

Transmitter Parameters		
T_1	Coordinate(m) (0,0,0)	Attitude angle(°) (0,0,0)
	Internal parameters: $\varphi_1 = 45°, \varphi_2 = -45°, \theta_{off} = -90°, \Delta z = 0.1$mm	
T_2	Coordinate(m) (10,0,0)	Attitude angle(°) (0,0,0)
	Internal parameters: $\varphi_1 = 45°, \varphi_2 = -45°, \theta_{off} = -90°, \Delta z = 0.1$mm	
T_3	Coordinate(m) (0,10,0)	Attitude angle(°) (0,0,0)
	Internal parameters: $\varphi_1 = 45°, \varphi_2 = -45°, \theta_{off} = -90°, \Delta z = 0.1$mm	
	Scanning angle error(")	$15 \times randn$ [a]
Receiver Coordinates [b]		
R_0 (5.0004, 2.0002, 1.0001)		R (5.0,2.0,1.0)

[a] The scanning angle error simulates the real working state, and "$randn$" stands for a random number with a mean of zero and a variance of one. The unit is angular second;
[b] "R" stands for the real coordinates of Receiver which is chosen at random. "R_0" stands for the initial coordinate of Receiver with a measurement error. The unit is meter.

In Fig. 9, there are three transmitters working from Time 1 to Time 39 and Time 71 to 100, and two transmitters working from Time 40 to Time 70. This simulates the process in which transmitters' number decreases from 3 to 2 and then increases back to 3. It can be seen from the test results that the positioning output of the two algorithms are not affected
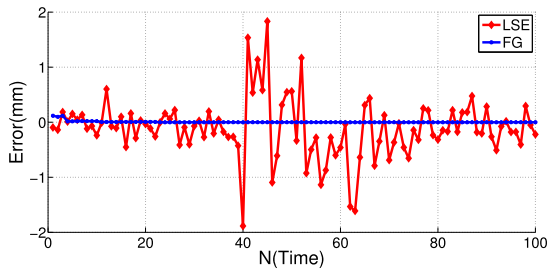
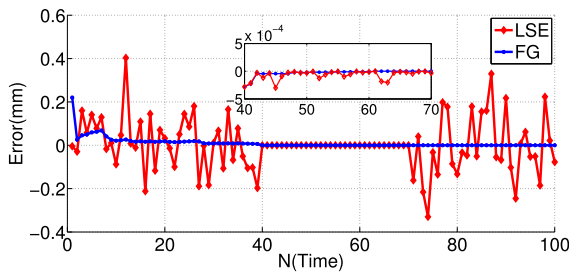**FIGURE 6.** A directed acyclic graph.
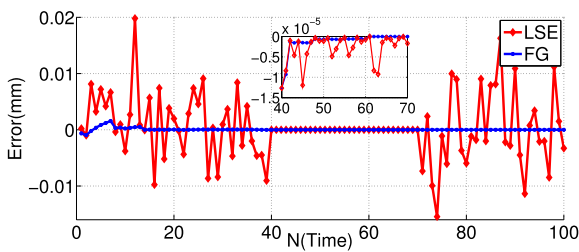

FIGURE 7. A directed acyclic graph.

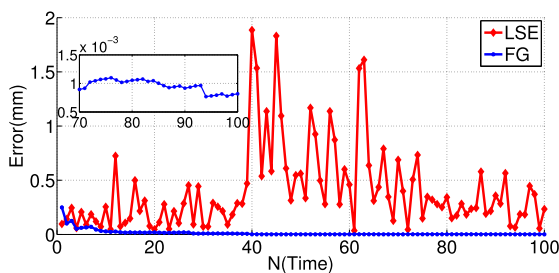**FIGURE 8.** A directed acyclic graph.

FIGURE 9. A directed acyclic graph.

by the change in the number of transmitters. It should be noted that for the LSE algorithm, the process of model selection is ignored during the whole simulation period. In other words, for the moment when the transmitters' number changes, the positioning results of the corresponding model at that moment are directly output.

According to the results, we can see that the positioning error based on FG does not jump significantly when the number of transmitters changes, however, the positioning error based on LSE has been affected dramatically when the positioning scheme changes. This shows a great plug-and-play performance for the positioning algorithm based on FG.

According to the four figures above, the positioning error based on FG is convergent in trend, but it is still influenced by the measurement information, such as Time 2 to Time 7 and Time 40 to Time 50 in Fig. 7 and Fig 8 and Time 70 to Time 100 in Fig. 6 and Fig. 9. However, the positioning error based on FG is not higher than the measurement error or the positioning error at the previous time. This is because the algorithm based on FG improves the correlation between the measurement information.

We can see the positioning error based on FG isn't disturbed by the gross errors such as Time 40 and Time 46 in Fig. 6, Time 12 in Fig. 7, which shows the proposed algorithm has very good robustness and stability. Besides, if the measurement information is quite good with a small error such as Time 4 in Fig. 6, Time 9 in Fig. 7 and Time 8 in Fig. 8, the positioning error will immediately approach to 0, which shows the algorithm based on FG makes full use of the optimal information. As a result, the accuracy has been further improved.

In summary, the experimental results show that the positioning effect of FG is better than that of LSE, what's more, the experimental results satisfy the theoretical analysis in Section 3, which shows the correctness of the theoretical analysis.

2) THE WHOLE SPACE POSITIONING EXPERIMENT

We have only chosen one random point to compare the effect of FG and LSE, which is not representative. In order to verify the accuracy of the proposed algorithm, this section discusses the positioning effect of the two algorithms in the whole measurement space.

The experiment conditions are the same as in Table 1, and We choose two transmitters' scheme, namely, T_1 and T_2. The whole measurement space is set as $10m \times 10m \times 10m$. We have carried 10 times simulation experiment. To compare the performance of these two algorithms, we randomly select one of the experiment, and the results are shown from Fig. 10 to Fig. 17.
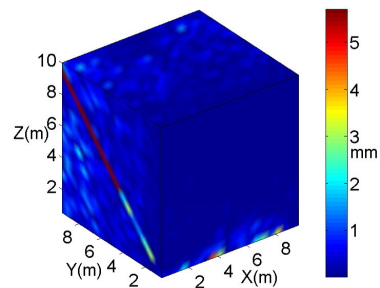

FIGURE 10. A directed acyclic graph.

The spots in the experimental figures are caused by the random variable of the scanning angle error. According to the figures above, we can clearly see that the positioning accuracy based on FG is better than that of LSE in the whole measurement, which shows the positioning algorithm based on
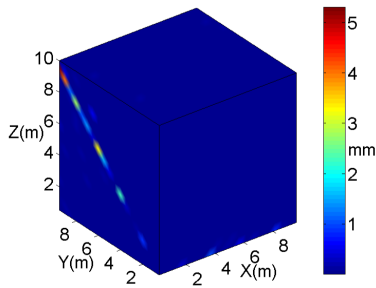
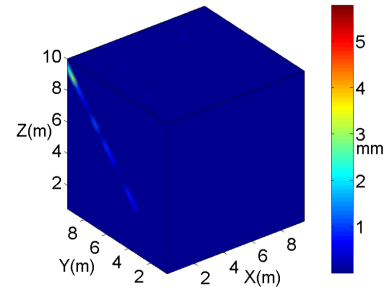**FIGURE 11.** A directed acyclic graph.
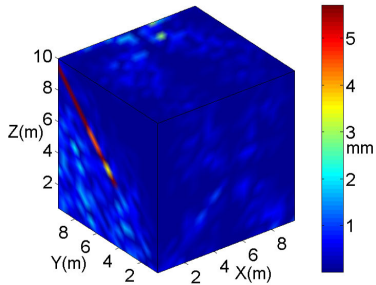

FIGURE 15. A directed acyclic graph.

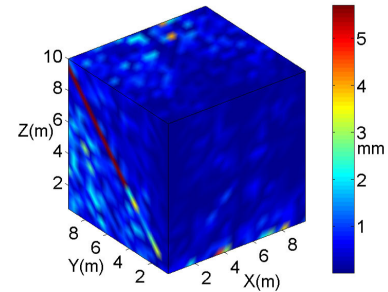**FIGURE 12.** A directed acyclic graph.

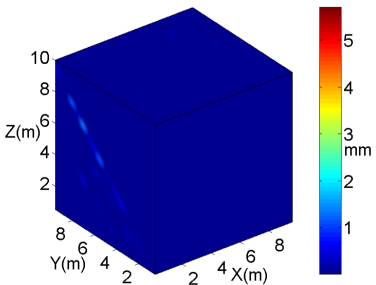**FIGURE 16.** A directed acyclic graph.

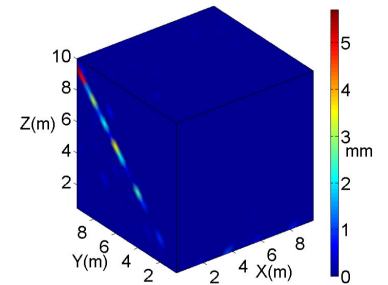**FIGURE 13.** A directed acyclic graph.

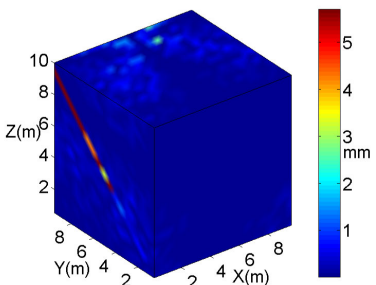**FIGURE 17.** A directed acyclic graph.
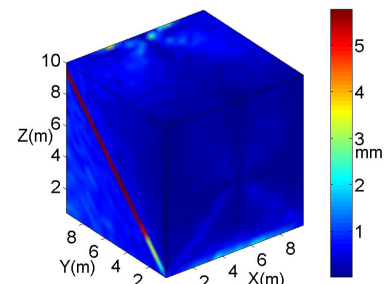

FIGURE 14. A directed acyclic graph.

FIGURE 18. A directed acyclic graph.

FG performs well in the whole measurement. Furthermore, we calculate the average of the ten positioning results of LSE, and the average total error of LSE is shown as Fig. 18. Comparing Fig. 16-Fig. 18, we can see that the proposed algorithm is still excellent.

There is an interesting thing in the figures above that needs further analysis, namely, there is an extreme value line in the plane of *Y-O-Z*, and the inclined angle of this line is

nearly 45°. Next, we will take Equation (18) as an example to study the formation of the extreme value line.

For the convenience of analysis, the parameters except φ_1 in Table 1 are substituted into Equation (18).

$$\boldsymbol{\mu}_{\boldsymbol{h}_{\boldsymbol{\theta}} \rightarrow \tilde{\boldsymbol{x}}_{\boldsymbol{k}}^{\boldsymbol{n-1}}} = - \left(-X \sin \theta_{x_k^{n-1}} \cos \varphi_1 - y \cos \theta_{x_k^{n-1}} \cos \varphi_1 \right.$$
$$\left. - z \sin \varphi_1 \right) \Big/ \left(\sin \theta_{x_k^{n-1}} \cos \varphi_1 \right) \quad (43)$$

(y, z) is the coordinates of the receiver to be measured at the previous time. X is the X-axis coordinate of T_2 in the global coordinate system, namely, $X = 10$. Thus the positioning error in X-axis can be got by Equation (44). X_{true} is the true value of the receiver in X-axis, and it's a constant.

$$\Delta X = \mu_{h_\theta \to \tilde{x}_k^{n-1}} - X_{true} \tag{44}$$

To find the extreme value, take the derivative of Equation (44), and let $\partial \Delta X \big/ \partial \theta_{x_k^{n-1}} = 0$.

$$y \cos \varphi_1 - z \sin \varphi_1 \sin \theta_{x_k^{n-1}} = 0 \tag{45}$$

When Plane1 scans into the *Y-O-Z* plane, $\theta_{x_k^{n-1}} = \frac{\pi}{2}$, $\tan \beta = \frac{z}{y}$, rewriting Equation (45) as follows:

$$\tan \beta = \frac{1}{\tan \varphi_1} \tag{46}$$

According to Equation (46), we know the tangent value of the inclined angle of the extreme value line and the tangent value of the plane inclined angle are reciprocal of each other. Since $\varphi_1 = \frac{\pi}{4}$, thus $\beta = \frac{\pi}{4}$. In conclusion, the inclined angle of extreme value line is proved.

According to the above analysis, it can be found that the positioning error may be related to the placement position of the receivers, and the positioning errors may be different for different positions in the measurement space. Since this problem is irrelevant to the topic of this paper, we do not discuss it in detail in this paper.

B. VERIFICATION EXPERIMENT

A system called ship high precision measuring and positioning system (SHPMPS) which is similar to iGPS in principle has been developed to verify the validity of the proposed algorithm. The whole experiment scenario is shown as Fig. 19. A SHPMPS with three transmitters and 4 receivers are placed randomly in the place to be measured. The transmitters' parameters and coordinate system parameters have been calibrated in advance, and the transmitters' coordinates in the global coordinate system are shown as Table 2. To compare the anti-interference ability of LSE and FG, the random perturbations are added to the transmitters during the whole experiment. The receivers coordinates are measured by a Leica AT403 laser tracker whose accuracy is $\pm 15\mu m + 6\mu m/m$ [30].The receivers' coordinates are shown as Table 2, and these coordinates are treated as the benchmark value. The rotate speed of the transmitters is set as 50 revolutions per second, thus there are 50 times measurement information output per second in theory. The experiment starts with two transmitters scheme(T_1 and T_2), and changes into three transmitters scheme at about 1 second, and the whole experiment lasts about 2.5 second. This is long enough to complete the measurement for a static point. The algorithms based on FG and LSE are both used to realize the coordinate measurement, and the total positioning results of the 4 receivers are shown as Fig. 20 to Fig. 23.

TABLE 2. The coordinate of the system (Unit: millimeter).

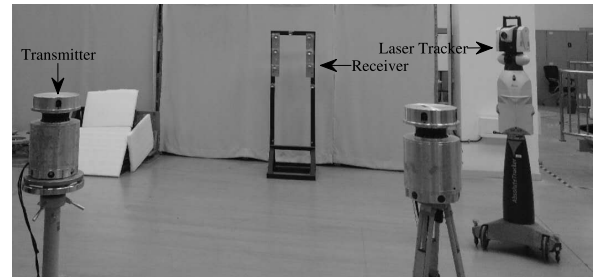| Transmitter	True Position	Receiver	True Position
T_1	(0.00,0.00,0.00)	R_1	(4849.02,10260.48,449.51)
T_2	(10151.02,0.00,48.98)	R_2	(5209.03,10123.52,459.48)
T_3	(12279.95,521.23,54.77)	R_3	(4869.02,10250.49,269.51)
		R_4	(5199.02,10140.52,294.48)

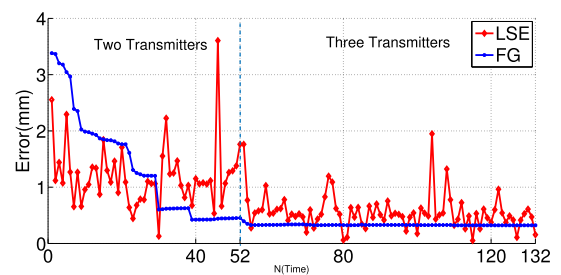**FIGURE 19.** A directed acyclic graph.

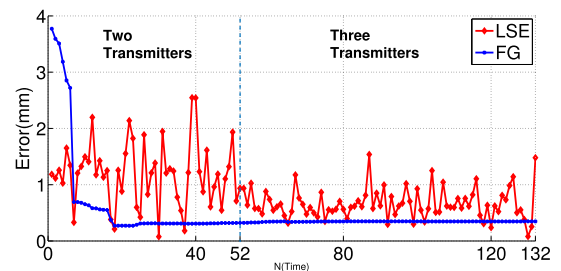**FIGURE 20.** A directed acyclic graph.

FIGURE 21. A directed acyclic graph.
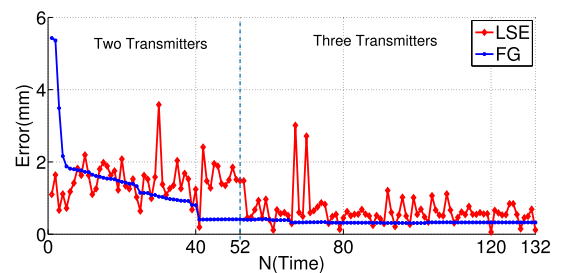

FIGURE 22. A directed acyclic graph.

According to Fig. 20-Fig. 23, 52 measurements have been made in the two-transmitters scheme and 80 in the three-transmitters scheme. The test results show that the system works well whether the transmitters' number changes or not. This verified that the change of the transmitters' number does not affect the positioning result output again.
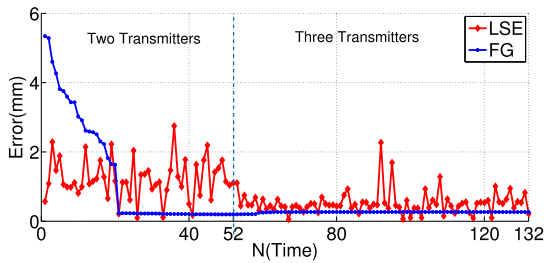
FIGURE 23. A directed acyclic graph.

TABLE 3. The average positioning error of receivers (Unit: millimeter).

Receiver	Algorithm	2 Transmitters		3 Transmitters	
		Average Error	Standard Error	Average Error	Standard Error
R_1	LSE	1.20	0.56	0.55	0.31
	FG	1.35	0.92	0.33	0.01
R_2	LSE	1.19	0.56	0.66	0.27
	FG	0.71	0.95	0.35	0.01
R_3	LSE	1.48	0.52	0.63	0.48
	FG	1.33	0.41	0.33	0.03
R_4	LSE	1.22	0.57	0.52	0.33
	FG	1.35	1.60	0.26	0.02

However, it should be noted that the positioning result of LSE in Time 52 and Time 53 are the same, this is caused by the change in the mathematical model of LSE. To ensure that there is a output at every moment, when the system does not work, we artificially take the result of the previous moment as the result output of this moment. On the grounds of the results above, we can get the following conclusions.

(1) The algorithm based on FG is more flexible than that of LSE. Due to the plug and play characteristics of the algorithm based on FG, when the number of the transmitters changes, the algorithm based on FG only needs to increase or decrease the computing nodes, which does not affect the algorithm's solution speed and output frequency. However, the algorithms based on LSE need to change the solution model, which will affect the solution efficiency, even it may cause the positioning results cannot be solved when there is no preset model in the algorithm. Such as the output in the 52nd and 53rd update.

(2) The proposed algorithm has higher accuracy. It is not difficult to see from the figures above that the proposed algorithm has higher accuracy compared with the traditional algorithm. Table 3 summarizes the average positioning error and standard error of the two algorithms under different transmitter scheme. It can be seen from the table that the accuracy of the proposed algorithm is improved by about 50% under the condition of the three-transmitters scheme, and the standard error in FG is much lower than that in LSE, which reflect the stability of the algorithm based on FG. As for the average positioning error of the proposed algorithm is not better than the traditional algorithm in the two-transmitters scheme, this is because the initial value errors of the proposed algorithm is too large, but as the number of iterations increases, the positioning error gradually stabilizes at a small amount (At this time, the error of the proposed algorithm is also smaller than that of the traditional algorithm), which reflects a good convergence of the proposed algorithm, also reflects the low requirement for the initial value of this algorithm. As a result, the calculation difficulty of the algorithm has been reduced.

(3) The stability of the proposed algorithm is much better. With the increase of the observation information, the proposed FG algorithm can quickly obtain a higher positioning accuracy through constant iteration, and in the subsequent process, the proposed FG algorithm is not subjected to the interference of outliers, thus the output is very stable. While the result of the LSE algorithm is very independent, its location accuracy is lower, and it has to bear the interference of outliers.

(4) The anti-interference ability is better for the proposed algorithm. The results in Fig. 20 compare the anti-interference ability of the two algorithms. For example, at Time 46, 76, 104, 108 in Fig. 20, the positioning results by LSE are significantly higher than those at other times, and the reason for these large errors is our random perturbations, however, the positioning results by FG have not been significantly affected. Thus the factor graph has better anti-interference ability than the LSE. Also the positioning results of Time 39, 40, 87,132 in Fig. 21, Time 30, 67, 70 in Fig. 22 and Time 36, 92, 95 in Fig. 23 can prove the better anti-interference ability of the factor graph.

In addition, there are two findings from the test results. One is that the positioning accuracy is significantly improved as the number of transmitters increase, and the other is that the positioning accuracy is various at different locations, which also corresponds to the simulation results.

V. CONCLUSION

This paper presents a novel 3D coordinate positioning algorithm based on factor graph suitable for iGPS under large scale conditions. Compared with the traditional least square method, the proposed algorithm has the characteristics of plug and play, good stability and high positioning accuracy. The proposed algorithm is no longer limited to a fixed mathematical model. By changing the number of factor graph nodes, a flexible solution of the positioning results is realized, making the algorithm easier to use.

Simulation experiments and prototype tests have proved that, compared with the traditional least square algorithm, the positioning accuracy of the proposed algorithm under the condition of three transmitters is improved by about 50%, and the highest positioning accuracy reaches about 0.3mm on average within 10 meters. At the same time, due to the good stability of the proposed algorithm, the confidence of the system output results is greatly improved. Thus the performance of the system has been optimized obviously.

This article only studies the application of factor graphs in iGPS, for other plug and play systems, we also believe that factor graph will also perform well. In the future, we will optimize the positioning algorithm based on factor graph

from the number of transmitters and layout of the receivers, which is not discussed in detail in this paper.

REFERENCES

[1] C.-M. Own, J. Hou, and W. Tao, "Signal fuse learning method with dual bands WiFi signal measurements in indoor positioning," *IEEE Access*, vol. 7, pp. 131805–131817, 2019.

[2] G. De Blasio, A. Quesada-Arencibia, C. R. Garcia, J. C. Rodriguez-Rodriguez, and R. Moreno-Diaz, "A protocol-channel-based indoor positioning performance study for Bluetooth low energy," *IEEE Access*, vol. 6, pp. 33440–33450, 2018.

[3] Y. Zeng, X. Chen, R. Li, and H.-Z. Tan, "UHF RFID indoor positioning system with phase interference model based on double tag array," *IEEE Access*, vol. 7, pp. 76768–76778, 2019.

[4] Y. Alvarez and F. Las Heras, "ZigBee-based sensor network for indoor location and tracking applications," *IEEE Latin Amer. Trans.*, vol. 14, no. 7, pp. 3208–3214, Jul. 2016.

[5] N. Bai, Y. Tian, Y. Liu, Z. Yuan, Z. Xiao, and J. Zhou, "A high-precision and low-cost IMU-based indoor pedestrian positioning technique," *IEEE Sensors J.*, vol. 20, no. 12, pp. 6716–6726, Jun. 2020.

[6] Q. Sun, Y. Tian, and M. Diao, "Cooperative localization algorithm based on hybrid topology architecture for multiple mobile robot system," *IEEE Internet Things J.*, vol. 5, no. 6, pp. 47–53, 2018.

[7] W. Guan, S. Chen, S. Wen, Z. Tan, H. Song, and W. Hou, "High-accuracy robot indoor localization scheme based on robot operating system using visible light positioning," *IEEE Photon. J.*, vol. 12, no. 2, pp. 1–16, Apr. 2020.

[8] W. Guan, Y. Wu, S. Wen, H. Chen, C. Yang, Y. Chen, and Z. Zhang, "A novel three-dimensional indoor positioning algorithm design based on visible light communication," *Opt. Commun.*, vol. 392, pp. 282–293, Jun. 2017.

[9] W. Guan, S. Wen, L. Liu, and H. Zhang, "High-precision indoor positioning algorithm based on visible light communication using complementary metal–oxide–semiconductor image sensor," *Opt. Eng.*, vol. 58, no. 2, Feb. 2019, Art. no. 024101.

[10] J. Liu, Q. Sun, and H. Cheng, "The state-of-the-art, connotation and developing trends of the products assembly technology," *J. Mech. Eng.*, vol. 54, no. 11, pp. 1–28, 2018.

[11] X. Sun, J. Bao, J. Li, Y. Zhang, S. Liu, and B. Zhou, "A digital twin-driven approach for the assembly-commissioning of high precision products," *Robot. Comput.-Integr. Manuf.*, vol. 61, pp. 1–14, Feb. 2020.

[12] Y. I. Wangmi, "Level docking technology in large cabin assembly," *Comput. Integr. Manuf. Syst.*, vol. 21, no. 9, pp. 2354–2359, 2015.

[13] L. I. Wupeng, X. Tian, J. Geng, D. Zhao, and M. Zhang, "Digital combined measuring technology of aircraft large components outline," *Aeronaut. Manuf. Technol.*, vol. 61, no. 8, pp. 80–84, 2018.

[14] J. Zhou, H. Xiao, W. Jiang, W. Bai, and G. Liu, "Automatic subway tunnel displacement monitoring using robotic total station," *Measurement*, vol. 151, Feb. 2019, Art. no. 107251.

[15] Y. Shi, "Study on the technology of determining the center line of shafting based-on laser theodolite," *J. Guangdong Commun. Polytech.*, vol. 16, no. 1, pp. 54–56, 2017.

[16] M. de Campos Porath, R. Simoni, R. de Araujo Nunes, and A. Bertoldi, "Feasibility of measurement-assisted assembly of ship hull blocks," *Mar. Syst. Ocean Technol.*, vol. 14, no. 1, pp. 23–33, Mar. 2019.

[17] J. E. Muelaner, Z. Wang, O. Martin, J. Jamshidi, and P. G. Maropoulos, "Verification of the indoor GPS system, by comparison with calibrated coordinates and by angular reference," *J. Intell. Manuf.*, vol. 23, no. 6, pp. 1–9, 2011.

[18] Y. Linghui, Z. Zhengji, L. Jiarui, W. Jinwang, and L. Bowen, "An overall shape measurement method for large components based on fusion of the optic-electrical scanning and positioning," *Infr. Laser Eng.*, vol. 48, no. 5, pp. 1–8, 2019.

[19] Z. Zhao, "Study on the dynamic measuring and positioning method and technique based on the wmps spatial measurement field," Ph.D. dissertation, Dept. Precis. Instrum. Optoelectron. Eng., TianJin Univ., Tianjin, China, 2016.

[20] L. Yang, "Research on large-scale space coordinate measurement location technology based on optical scanning," Ph.D. dissertation, Dept. Precis. Instrum. Optoelectron. Eng., TianJin Univ., Tianjin, China, 2010.

[21] S. Fan, Y. Zhang, Q. Hao, P. Jiang, C. Yu, and F. Yu, "Cooperative positioning for multi-AUVs based on factor graph and maximum correntropy," *IEEE Access*, vol. 7, pp. 153327–153337, 2019.

[22] S. Fan, Y. Zhang, C. Yu, M. Zhu, and F. Yu, "An advanced cooperative positioning algorithm based on improved factor graph and sum-product theory for multiple AUVs," *IEEE Access*, vol. 7, pp. 67006–67017, 2019.

[23] J. Luo, P. Xu, N. Pan, P. Jiang, X. Li, and H. Zhang, "Non-landing vehicle mounted electro-optical theodolite deformation measurement method using inertial sensors," *Meas. Sci. Technol.*, vol. 30, no. 5, 2019, Art. no. 055103.

[24] D. Lao, "Research on transmitter optimization and calibration technology of indoor measurement positioning system," Ph.D. dissertation, Dept. Precis. Instrum. Optoelectron. Eng., TianJin Univ., Tianjin, China, 2011.

[25] F. R. Kschischang, B. J. Frey, and H.-A. Loeliger, "Factor graphs and the sum-product algorithm," *IEEE Trans. Inf. Theory*, vol. 47, no. 2, pp. 498–519, Feb. 2001.

[26] A. Gupta and B. S. Rajan, "Reduced complexity sum-product algorithm for decoding nonlinear network codes and in-network function computation," in *Proc. IEEE Int. Conf. Commun.*, Apr. 2016, pp. 4070–4082.

[27] W. Zhao, "Research on multi-source fusion positioning theory and method," Ph.D. dissertation, Dept. Electron. Inf. Eng., Harbin Inst. Technol., Harbin, China, 2018.

[28] Z. P. Song and F. O. Mathematics, "Calculate the mean and the variance of continuous random variable by using Taylor's series," *Yinshan Academic J.*, vol. 21, no. 244, pp. 564–566, 2015.

[29] H. Qiang, Y. Hongliang, X. Dingjie, and Z. Bo, "Research on the IGPS device error and its influence of positioning accuracy," in *Proc. Forum Cooperat. Positioning Service (CPGPS*, May 2017, pp. 294–299.

[30] M. Luo, T. Wang, L. Dong, and T. Luo, "Research on the error analysis and calibration method of the theodolite and laser ranger combination system," *Metrology Meas. Technol.*, vol. 38, no. 4, pp. 20–25, 2018.

QIANG HAO was born in 1992. He received the B.S. degree from the Department of Automation, Harbin Engineering University, Harbin, China, in 2015. He is currently pursuing the Ph.D. degree in instruments science and technology with the Harbin Institute of Technology. His current research interests include inertial navigation systems and indoor positioning systems.

YA ZHANG received the B.Eng. and Ph.D. degrees from Harbin Engineering University, Harbin, China, in 2010 and 2015, respectively. She is currently holding a postdoctoral position with the School of Instrumentation Science and Engineering, Harbin Institute of Technology, Harbin, Heilongjiang. Her current research interests include vision-based mobile robot navigation systems and multi-sensor information fusion.

SHIWEI FAN was born in 1993. He received the B.S. degree from the Department of Automation, Harbin Engineering University, Harbin, China, in 2015. He is currently pursuing the Ph.D. degree in instruments science and technology with the Harbin Institute of Technology. His current research interests include inertial navigation systems and cooperative navigation systems.

PAN JIANG was born in 1993. He received the bachelor's degree from Harbin Engineering University, China, in 2015. He is currently pursuing the Ph.D. degree with the Harbin Institute of Technology. His main research interest includes high precision inertial navigation algorithm.

DINGJIE XU was born in 1966. He is currently a Professor and a Ph.D. Tutor with the Institute of Navigation Instrument, Harbin Institute of Technology. He is mainly engaged in teaching and research in navigation, guidance, and control.

● ● ●

HONGLIANG YIN was born in 1984. He received the Ph.D. degree from Beihang University, Beijing, China, in 2013. He is currently a Senior Engineer with the China Ship Research and Development Academy. His main research interest includes high precision inertial navigation algorithm.